Photon Energy Upconverting Nanopaper: A Bioinspired Oxygen Protection Strategy

Anna J. Svagan,[†,‡,*] Dmitry Busko,[‡] Yuri Avlasevich,[‡] Gunnar Glasser, Stanislav Baluschev,[§,*] and Katharina Landfester[*]

Max Planck Institute for Polymer Research, Ackermannweg 10, 55128 Mainz, Germany. [‡]These authors contributed equally. [†]Present address: Department of Food Science, University of Copenhagen, Rolighedvej 30, 1958 Fredriksberg C, Denmark. [§]Present address: Optics and Spectroscopy Department, Faculty of Physics, Sofia University "St. Kliment Ochridski", 5 James Bourchier, 1164 Sofia, Bulgaria.

ABSTRACT The development of solid materials which are able to upconvert optical radiation into photons of higher energy is attractive for many applications such as photocatalytic cells and photovoltaic devices. However, to fully exploit triplet−triplet annihilation photon energy upconversion (TTA-UC), oxygen protection is imperative because molecular oxygen is an ultimate quencher of the photon upconversion process. So far, reported solid TTA-UC materials have focused mainly on elastomeric matrices with low barrier properties because the TTA-UC efficiency generally drops significantly in glassy and semicrystalline matrices. To overcome this limit, for example, combine effective and sustainable annihilation upconversion with exhaustive oxygen protection of dyes, we prepare a sustainable solid-state-like material based on nanocellulose. Inspired by the structural buildup of leaves in Nature, we compartmentalize the dyes in the liquid core of nanocellulose-based capsules which are then further embedded in a cellulose nanofibers (NFC) matrix. Using pristine cellulose nanofibers, a sustainable and environmentally friendly functional nanomaterial with ultrahigh barrier properties is achieved. Also, an ensemble of sensitizers and emitter compounds are encapsulated, which allow harvesting of the energy of the whole deep-red sunlight region. The films demonstrate excellent lifetime in synthetic air (20.5/79.5, O_2/N_2)—even after 1 h operation, the intensity of the TTA-UC signal decreased only 7.8% for the film with 8.8 μm thick NFC coating. The lifetime can be further modulated by the thickness of the protective NFC coating. For comparison, the lifetime of TTA-UC in liquids exposed to air is on the level of seconds to minutes due to fast oxygen quenching.

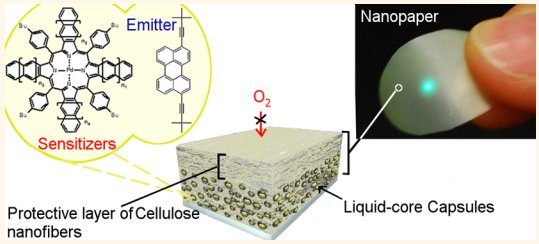

KEYWORDS: triplet−triplet annihilation upconversion · solid-state-like · nanofibrillated cellulose · cellulose nanocrystals · low oxygen permeability · bioinspired

Photon energy upconversion (UC) is an assembly of inter- and intramolecular processes in which the low energy of multiple photons is harnessed and recombined into a single photon of higher energy. Upconversion by triplet−triplet annihilation (TTA) was recently extended to ultralow intensity of noncoherent excitation light (less than 10 mW cm^{-2}), corresponding to the solar intensity at the Earth's surface.[1−3] Such low-energy requirements allow the development of several unique applications in material science,[4−17] solar cell devices,[18] solar fuels,[19] and bioimaging.[20−26] However, to fully exploit the TTA-UC process in different applications, the importance of the development of solid-state-like TTA-UC materials for better device integration cannot be neglected: such materials are easily processable. Even more, building an effective protection mechanism against quenching by molecular oxygen and protection against the subsequent production of highly reactive singlet oxygen is imperative for long lifetime and efficient TTA-UC processes in ambient environments.

Recently, several unique upconverting solid-state materials have been reported based on "photophysically" inert matrices such as ethylene oxide/epichlorohydrin copolymer,[2] poly(ethylene glycol),[27] polyurethane,[16,28] polyacrylates,[29] poly(methyl methacrylate),[30−32] cellulose acetate,[33] and styrene/divinylbenzene/vinylbenzyl chloride copolymer.[34] Also some solid-state-like materials, in the form of capsules, have been reported which contain oil or dissolved polymer with unsaturated double bonds that chemically quench the singlet oxygen.[20,35,36] In the case of solid-state materials, the main

* Address correspondence to landfest@mpip-mainz.mpg.de, balouche@phys.uni-sofia.bg, wzn206@ku.dk.

Received for review May 7, 2014 and accepted July 14, 2014.

Published online July 14, 2014
10.1021/nn502496a

focus has been matrix polymers with low glass transition temperatures (*e.g.*, rubbery materials) to obtain high-efficiency solid-state systems. The larger upconversion efficiency for such materials, when compared to glassy/rigid materials, has been theorized to be due to higher segmental mobility of the elastomers and also enhanced local molecular mobility of the chromophores, which increases interaction probability and thus energy transfer and TTA processes.[29,37] Difference in dye solubility is another plausible explanation.[30] Note that upconversion phenomena are not precluded by glassy polymers, but the efficiency is much lower.[29] However, irrespective of the governing mechanism, more importantly, the oxygen barrier properties of the solid-state films are missing or never discussed for the referenced systems. In the case of rubbery materials, low oxygen barrier properties are anticipated, due to the high free volume associated with such materials.[38,39] Hence more research on upconverting solid-state materials is needed in order to fulfill the imperative requirements for effective and sustainable annihilation upconversion combined with exhaustive oxygen protection of the UC chromophores.

Cost-efficient and environmentally friendly functional nanomaterials based on materials from renewable resources has gained substantial attention during recent years. In particular, cellulose nanofibers (NFC) are regarded as one of the most promising bioderived materials due to the extraordinary set of physical properties, such as outstanding mechanical properties (100−160 GPa for the crystal modulus), optical transparency, nontoxicity, and ultrahigh oxygen barrier properties.[40−50] The oxygen barrier properties of pristine NFC films are about 2−3 orders of magnitude better than the best petrochemically derived polymer, ethylene vinyl alcohol (23 °C, 0% RH). The high barrier properties are a consequence of the semicrystalline structure and optimal packing of nanocellulose in pristine films.[47,50] Cellulose nanofibers, in the form of microfibrils (width ∼3 nm), are the principal scaffolding component in plants.[51]

Herein, NFC was exploited in the making of a solid-state-like upconverting material. Direct mixing of NFC with chromophores was however not possible because, due to its hydrophilic nature, NFC tends to aggregate in most nonpolar "solvents" (or polymers), making it difficult to obtain well-dispersed systems. Therefore, an original concept for designing a solid-state-like TTA-UC film with high oxygen protective properties is presented. Nanocellulose-based capsules containing chromophores in the liquid core were prepared and successfully compounded with NFC. The inspiration for the design is the structural buildup of leaves in Nature[51] (compare Figure 1a,b). The scaffold for our "synthetic leaf" is much simpler, yet the main idea behind it is preserved: to compartmentalize the optically active molecules in liquid-core compartments (nanocellulose-based capsules in our case, chloroplasts in plant cells in natural leaves) and to regulate/hamper oxygen flow in order to gain effective and sustainable "light harvesting". Furthermore, in parallel with the natural leaves, our synthetic UC-leaf maximizes the harvesting of incident light by collecting a broad spectral range of low-intensity noncoherent excitation light, using a sensitizer ensemble of five different sensitizers (Figure 1b and Supporting Information Figure S1). Such nanocellulose-based liquid-core capsules embedded in pristine NFC films with upconverting abilities are new and have not been reported before.

RESULTS AND DISCUSSION

The upconversion process takes place in multichromophore systems consisting of energetically optimized pairs of sensitizer and emitter molecules, as shown in Figure 1c.[4−16] The photon energy is absorbed by a sensitizer and efficiently transferred in its triplet state *via* a process of intersystem crossing (ISC; see Figure 1c), strongly enhanced by the coordinated heavy atom (Pd). Further, this triplet energy is transferred to an emitter triplet and stored there (the emitter triplet states are metastable) *via* the process of triplet−triplet transfer (TTT). Next, the excited triplet states of two emitter molecules undergo triplet−triplet annihilation (TTA), in which one emitter molecule returns back to its singlet ground state and the other molecule gains the energy of both triplet states and is excited to the higher singlet state. As the singlet state emitter decays radiatively back to the ground state, a fluorescence photon is emitted which is strongly (blue) shifted to shorter wavelengths in relation to the excitation photons. The efficiency is greatly influenced by the presence of molecular oxygen (quencher), which effectively depopulates the triplet states of the sensitizer, and oxygen is therefore regarded as the most critical contaminant.[52] In Figure 1c, the energetic scheme for the TTA-UC process in the multicomponent organic system in the presence of molecular oxygen is presented. It is important to notice that in an oxygen-saturated environment the probability to relax the excited triplet state of the sensitizer *via* generation of singlet oxygen (marked with the brownish circle) is much higher than that toward the triplet state of the emitter. Therefore, in an oxygen-saturated environment, the TTA-UC process is completely quenched. Additionally, the singlet oxygen is a highly reactive species, which accelerates the photo-oxidation of the UC dyes. In an oxygen-free environment, the TTA-UC follows the previously described mechanism.[1−3]

By encapsulation the UC dyes in the liquid compartment of micro/submicron-sized nanocomposite shell/liquid core capsules, the local mobility of the chromophores is maintained. The shell wall of the capsules is

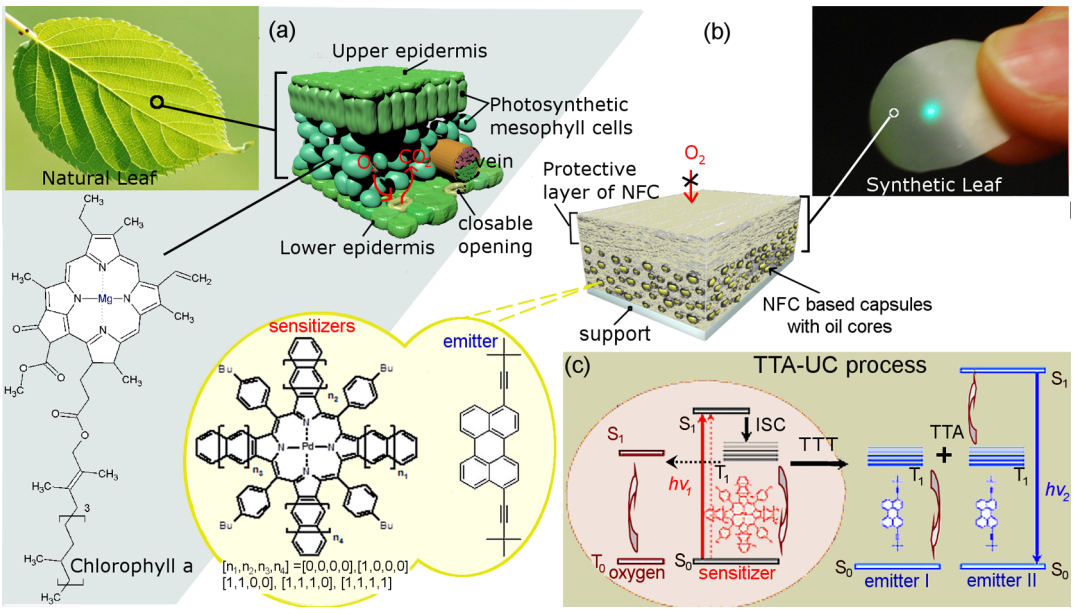

Figure 1. (a) Structural buildup of a natural leaf, showing the protective outer epidermis layers and the closable openings through which the flow of CO_2 and O_2 is regulated. Between the epidermis layers, the liquid-filled parenchyma cells (palisade and spongy mesophyll) are found. The chlorophyll is present in the chloroplasts that are found within the mesophyll cells. (b) Structure of the synthetic leaf showing the (high oxygen barrier) protective layer of cellulose nanofibers and the embedded oil-core capsules underneath. The sensitizers and emitter are present in the liquid cores of the capsules. The cyan dot on the synthetic leaf is the UC emission obtained at broad-band excitation. The synthetic leaf (inset) was decoupled from its underlying support. The scattered excitation radiation is blocked by a short pass filter (SP01-633RU-25, Semrock Inc.). (c) Simplified scheme for the TTA-UC process in multicomponent organic systems and quenching of the TTA-UC process (the brownish circle) in the presence of molecular oxygen.

armored with a blend of semicrystalline cellulose nanofibers/cellulose nanocrystals, and the liquid core consists of hexadecane (Figure 2a, close-up in Supporting Information, Figure S3). NFCs are long flexible nanofibers composed of both crystalline and amorphous regions, whereas cellulose nanocrystals (CNC) are shorter, rod-like mainly crystalline whiskers. These capsules are then further embedded in a matrix of NFC which supplies the necessary mechanical support. Also, both capsule shell and matrix material decrease the oxygen permeability, following the strategy of a tortuous path for the oxygen molecules around the impermeable crystalline parts of the semicrystalline nanocellulose used in the capsule shell and matrix material.[47,53−55]

In Figure 2a (and Figure S3), typical nanocellulose-based capsules containing oil (hexadecane) cores are presented, where the fibrous capsule wall structure is clearly resolved. The capsule wall was created by the reaction between the hydroxyl groups of NFC/CNC, cross-linker (isophorone diisocyanate), and water at the oil/water interface of oil droplets (see Scheme 3 in the Methods section). A blend of NFC and CNC was used in the capsule synthesis. The NFC/CNC blend was prepared using a new hydrolysis route from wood pulp, as described previously.[56] Additionally, apart from becoming an integral part of the capsule shell wall, the NFC/CNC also stabilized the oil/water interface during the capsule synthesis *via* a Pickering mechanism.[57] NFC/CNC was used in the capsule synthesis in order to gain an optimal matrix/capsule wall adhesion in the films and eliminate the need for additional surfactant which could potentially harm film formation properties and hence the oxygen barrier properties of the resulting nanocomposite.[47] The capsules were on average $1.2 \pm 0.3\ \mu$m in diameter, with a capsule wall thickness of around 30 nm (Supporting Information, Figure S4). The concentration of sensitizer and emitter, present in the oil core of the capsules only, was 7×10^{-5} and 1×10^{-3} M, respectively. The capsules were blended with an additional amount of anionically charged NFC prepared by 2,2,6,6-tetramethylpiperidine-1-oxyl (TEMPO)-mediated oxidation. The TEMPO-NFC (2.98 ± 1.5 nm in diameter and 200−1000 nm in length, AFM image in Figure 2b) binds the capsules together, forming the solid-state film. In natural leaves, the gas flow is regulated by the epidermis layer (see Figure 1a).[51] Inspired by this, we created an additional transparent layer of TEMPO-NFC on top of the capsule film in order to provide an effective oxygen barrier. By altering the thickness of this protective layer, the rate of gas transport to the capsules can be regulated. In Figure 2, a schematic overview of the resulting film (2d) and a scanning electron microscopy (SEM) image of a typical cross section of such film (2c) are presented, clearly displaying the two different layer types. The cross section for the SEM analysis was prepared by simple fracture in liquid nitrogen. The upper layer consists of a

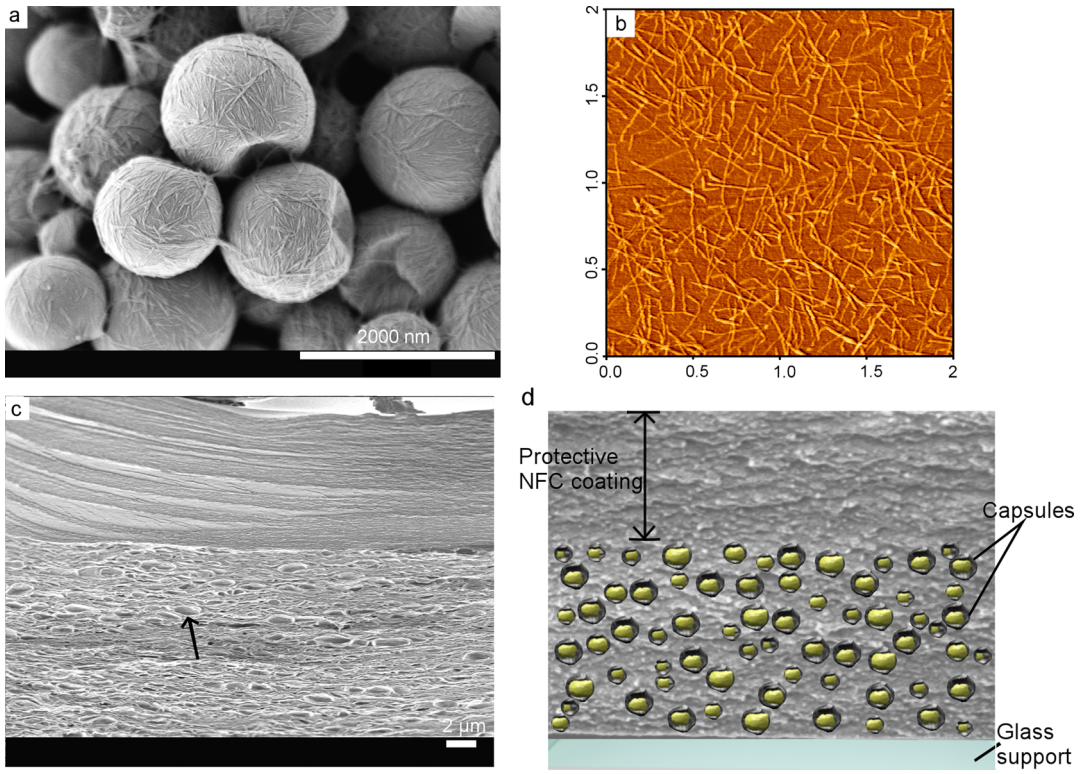

Figure 2. (a) SEM image of NFC/CNC-based capsules containing oil-liquid cores. The scale bar is 2 μm. The concentrations of dyes used are 1×10^{-3} M of emitter and 7×10^{-5} M of sensitizer. (b) AFM image of individual TEMPO-NFC (2.98 ± 1.5 nm in diameter and 200−1000 nm in length) used as matrix material and for the protective coating. The sides of the image are 2 μm. (c) Fracture surface of the synthetic leaf (SEM image) showing the two-layer structure, which consists of an upper protective coating and a lower part containing the capsules (arrow). The scale bar is 2 μm. (d) Illustration of the cross section of the synthetic film.

laminar structure of random-in-the-plane sheets of cellulose nanofibers.[58] This structure is markedly different from the underlying structure, where cross-sectioned capsules are clearly resolved. These capsules have to some extent been compressed during the film preparation; see Methods section for details on the preparation. The resulting nanocomposite was semi-transparent (see synthetic leaf (film) in Figure 1). By utilizing smaller capsules, the transparency could be further improved, however, unfortunately at the expense of the oxygen barrier properties due to an unfavorable increase of the surface-to-volume ratio. Nonetheless, it should still be possible to further optimize such parameters for the application of interest.

As stated previously, our synthetic UC-leaf maximizes the harvesting of incident light by collecting a broad spectral range of low-intensity noncoherent excitation light, using a sensitizer ensemble of five different sensitizers, as depicted in Figures 1b and 3a. The additive impact on the efficiency of the TTA-UC when using an ensemble of sensitizers has been demonstrated previously.[8] As shown in Figure 3a, the integral Q-band of the used sensitizer ensemble is much broader than the absorption band of each single sensitizer, thus it allows harvesting of the whole deep-red spectral region of terrestrial sunlight (spectral width $\Delta\lambda \sim 70$ nm) ranging from $\lambda = 620$ nm up to $\lambda = 690$ nm (measured at full width and half-maximum, fwhm). The usage of a sensitizer ensemble with optimized spectral range delivers more excitation photons capable for TTA-UC process harvested at a particular sunlight intensity; therefore, the required concentration of the sunlight can be substantially lowered. The absorption spectrum of each solitary sensitizer is reported in the Supporting Information (Figure S2b). The search of new deep-red and even IR absorbing sensitizer molecules is crucial because it can drastically increase the technological relevance of the TTA-UC process.[59,60]

As a singlet emitter, a π-extended perylene dye (3,9(10)-bis(3,3-dimethylbutyn-1yl)perylene) was used. The fluorescence spectral maximum (the green line in Figure 3c) of this emitter molecule is situated optimal into the transparency window of the sensitizer ensemble, thus the reabsorption of the UC emission is almost avoided. Comparison with the sensitizer ensemble absorption (shown in Figure 3a, brown line) demonstrates only small spectra overlapping at around $\lambda =$ 580 nm. The characteristic luminescence spectrum of the studied UC system excited with broad-band light is shown in Figure 3b. As expected, in oxygen-free atmosphere (oxygen contamination less than 2 ppm) and low excitation intensity, the UC fluorescence is very stable;

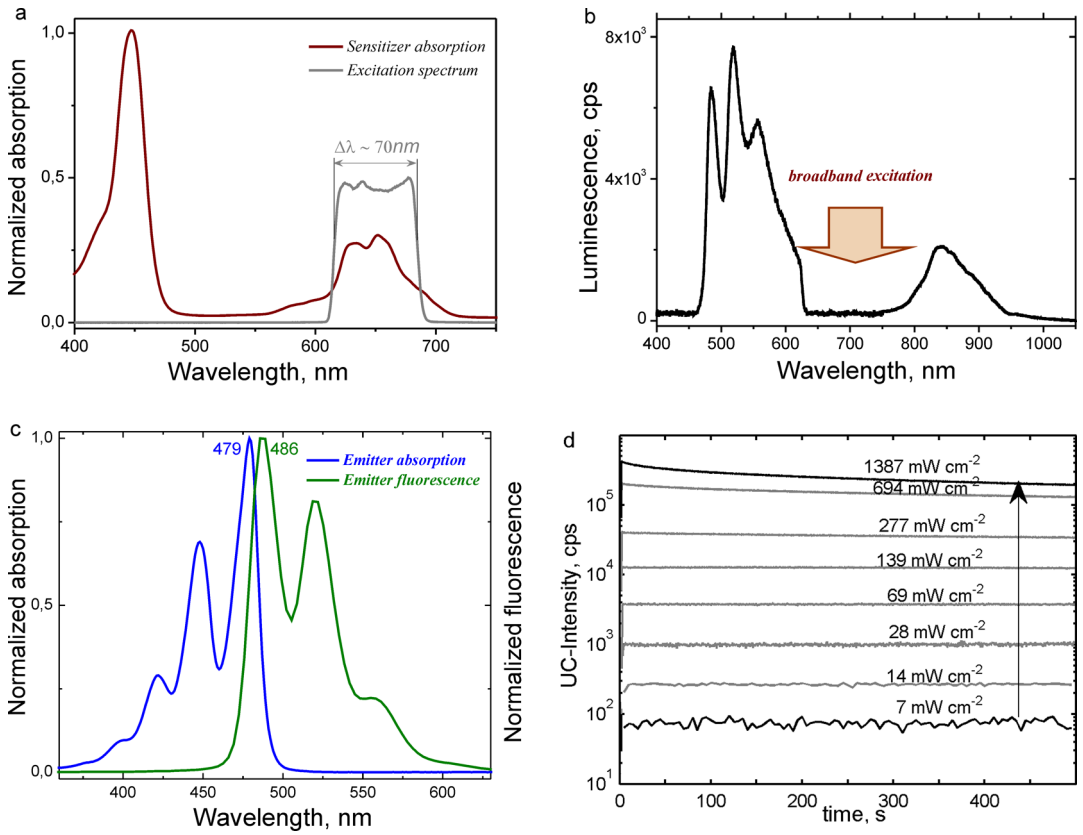

Figure 3. (a) Normalized absorption spectrum of sensitizer ensemble and the utilized broad-band excitation spectrum, $\Delta\lambda \sim 70$ nm (fwhm, $\Delta\lambda \sim 620-690$ nm). (b) Luminescence spectrum for the solid-state-like film subjected to broad-band excitation in the UC regime. (c) Normalized absorption spectrum (blue line) and the fluorescence spectrum (green line) of the emitter in toluene, emitter concentration 1×10^{-6} M. (d) UC fluorescence intensity ($\lambda_{max} = 518$ nm) in films as a function of different intensity of incident light ($\lambda = 639$ nm) in nitrogen atmosphere (<2 ppm of O_2).

especially, for intensities lower than 500 mW cm^{-2} even at long observation periods (in order of 500 s), no change of the UC efficiency in oxygen-free atmosphere is observed (Figure 3d). At these conditions, the quantum yield (defined in classical meaning)[11] of the solid-state-like NFC protective film, embedding liquid-core capsules with the studied UC system was estimated to be 8.2% at broad-band excitation (light intensity ~500 mW cm^{-2}, excitation spectrum shown in Figure 3a, the gray line).

Herein, three different types of films were prepared: one without and two with protective coatings of different thicknesses, namely, 4.2 and 8.8 μm (see Figure 2c,d). The thickness of the lower capsule layer was comparable for the three film types and is on the order of 29 $\pm$ 3 (films with protective coatings) to 36.5 μm (reference film). All films were supported on glass substrates (Petri dishes; see Methods section for preparation details). These samples were equilibrated in a nitrogen atmosphere and then exposed to dry synthetic air (20.5/79.5 vol %, O_2/N_2, constant and identical temperature for the synthetic air and sample), with the oxygen permeation schematically depicted in Figure S5. The change in intensity (I) of the generated emission was monitored with time. The results in Figure 4a,b show the normalized UC fluorescence and phosphorescence intensity, respectively, where the inlet of synthetic air is marked with an arrow. The intensities (I) were normalized by dividing with the intensity prior to oxygen inlet (I_0). In all cases, the intensity declines as more oxygen penetrates through the structure and effectively quenches the excited triplet states of the chromophores. As expected, the UC fluorescence decreased more rapidly than the phosphorescence signal.[61] The explanation for this behavior is the fact that UC fluorescence is a consequence of the bimolecular TTA process. Both sensitizer and emitter excited triplet ensembles can be quenched by molecular oxygen; therefore, the UC fluorescence demonstrates stronger dependence on the oxygen concentration. Even more, the oxidation of the active dyes cannot be neglected if large observation times (on the order of hours of noninterrupted optical pumping, reported in Figure 4) are used. This oxidation leads to a substantial decrease of the molecular concentration of the sensitizer and emitter molecules, participating in the TTA-UC process and further decreases the stability of the UC fluorescence during the excitation in ambient conditions.

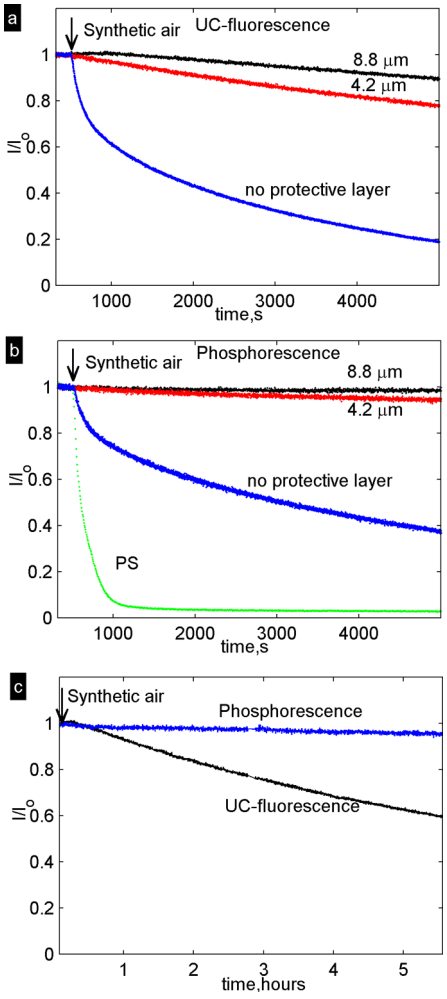

Figure 4. Normalized UC fluorescence at λ_{max}= 518 nm (a) and normalized phosphorescence at λ_{max}= 831 nm (b) as a function of time (s) in a NFC-based film with no additional protective layer (blue) and 4.2 μm (red) or 8.8 μm (black) thickness of the oxygen protective layer. The intensities (I) were normalized by dividing with the intensity prior to air inlet (I_0). The curves are an average of three measurements. In (b), the phosphorescence (green) of a polystyrene (PS) film (single measurement) is also included, which contains the same concentration of sensitizer/emitter as in the liquid phase of capsules. No UC fluorescence was observed for the PS film. The time of inlet of the synthetic air (20.5/79.5, O_2/N_2) is marked in the respective plot. In (c), a long-time experiment (>5 h) is also presented for the film with an 8.8 μm thick protective layer. These curves are an average of two measurements. All experiments were performed in a dry atmosphere at a constant temperature of 26.3 $\pm$ 0.8 °C at 1050 mbar. The samples were excited at λ = 639 nm (at an intensity of 139 mW cm^{-2}). As shown in Figure 3d, for low intensities (<500 mW cm^{-2}) and oxygen-free atmosphere, UC signal is stable for long observation periods.

For films with protective coatings, a delay between the synthetic air inlet and UC emission drop was noted, simply because the oxygen needs to penetrate the protective coating before it can start quenching the excited triplet states. The slopes of the curves decrease with increasing thickness of the coating. In Figure 4c, a long time experiment (more than 5 h) is presented for the film type with thickest protective coating. Within this time scale, the normalized UC fluorescence dropped around 40%, whereas the normalized phosphorescence decreased only slightly.

To further demonstrate the oxygen protective properties of NFC-based films, a comparison was made to a polystyrene film containing directly embedded UC chromophores and with a film thickness of 51.6 $\pm$ 2.3 μm (see Figure 4b). The concentration of sensitizer/emitter in the PS film was the same as in the liquid phase of NFC-based films. Soft polymers have previously been used in the fabrication of upconverting polymer films.[6] For these films, the quantum yield of the UC fluorescence decreases dramatically in comparison with the UC quantum yield of the same UC systems, but dissolved in liquid solvent. The main reason is the low molecular mobility of the chromophores. As shown in Figure 4, the UC fluorescence of those films (at the corresponding excitation conditions, intensity of 139 mW cm^{-2}) is not observed, and the registered residual phosphorescence of a PS film is also quickly quenched (green line of 4b) in an oxygen-rich atmosphere. This is anticipated since the oxygen permeability in polystyrene is more than 6 orders of magnitude higher than for NFC.[50] UC fluorescence can be achieved in PS matrices but will depend on factors such as the intensity of the incident light, dye concentration, and molecular mass of the PS.[37,62]

The reported oxygen permeability coefficient for TEMPO-NFC-based films in literature is 0.0008 mL (STP) μm m^{-2} day^{-1} kPa^{-1} at 23 °C and 0% RH.[47] To verify that our protective coating has an oxygen permeability coefficient in the right order of magnitude, a solvent-cast neat TEMPO-NFC film was prepared and tested with an OPT tester. In this case, the value obtained was below the measurement limit of the machine, that is, <0.001 mL (STP) μm m^{-2} day^{-1} kPa^{-1} at 23 °C and 20% RH, which strengthens the conclusion that our films exhibit low oxygen permeability and thus considerable protecting effect.

CONCLUSIONS

A bioinspired upconverting solid-state-like film was successfully synthesized for the first time using nanocellulose in both capsule wall formation and as film matrix material. An ensemble of asymmetrically annelated sensitizers and energetically optimized emitter was encapsulated, which allows harvesting of the energy of the whole deep-red sunlight region. The films demonstrated excellent lifetime and efficient upconversion in an oxygen-saturated environment, due to delayed quenching processes of oxygen and high local mobility of the chromophores. The lifetime can be further modulated and increased by introducing thicker protective cellulose nanofiber coatings. Effective oxygen protection is imperative for efficient

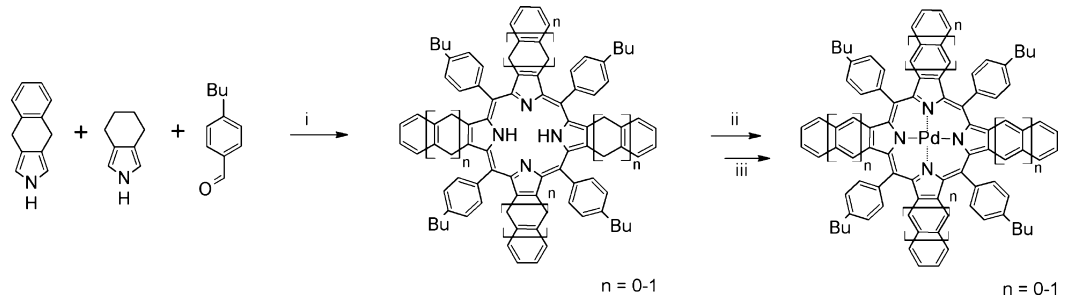

Scheme 1. Reagents and conditions: (i) $BF_3 \cdot Et_2O$, dichloromethane, DDQ, room temperature; (ii) $Pd(PhCN)_2Cl_2$, Et_3N, THF, reflux; (iii) DDQ, THF, reflux.

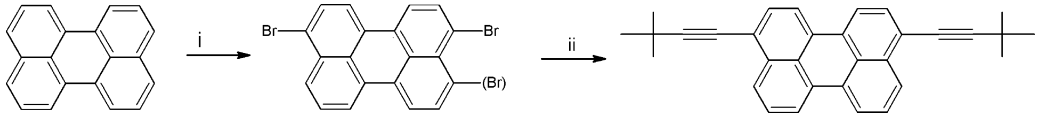

Scheme 2. Reagents and conditions: (i) Br_2, AcOH; (ii) 3,3-dimethylbutyne, $Pd(PPh_3)_4$ (100 mg) and CuI, THF, piperidine.

and sustainable annihilation upconversion and of immense importance for successful device integration. Furthermore, cellulosic nanofibers are sustainable, biodegradable, and derived from an inexhaustible plant source, hence paving the way for the creation of a fully recyclable and inexpensive TTA-UC solid-state-like film.

METHODS

Materials. The solvents and chemicals used were of commercial grade. Never-dried bleached sulfite pulp from spruce was used as the source for the NFC/CNC (kind gift from Nordic Paper Seffle AB, Säffle, Sweden). The pulp contains 13.8 wt % hemicellulose and 0.7 wt % lignin.

Synthesis of Porphyrin Mixture *via* the Lindsey Method (Scheme 1). The synthesis scheme of a novel porphyrin mixture, containing Pd-porphyrins with different number of benzo and naphtho units (Scheme 1 and Figure S1), was similar to that of Niedermair *et al.*[63] with the major modification that 4-butylbenzaldehyde was used instead of 4-fluorobenzaldehyde. 4,5,6,7-Tetrahydroisoindole (72 mg, 0.059 mmol, 0.5 equiv) and 4,9-dihydro-2*H*-benz[*f*]isoindole (100 mg, 0.059 mmol, 0.5 equiv) were dissolved in dry CH_2Cl_2 (100 mL). The tetrahydroisoindole and benzodihydroisoindole were synthesized as described before.[63] The reaction mixture was degassed for 20 min with N_2. The stirred mixture was protected from light and stirred under N_2. 4-Butylbenzaldehyde (192 mg, 0.118 mmol, 1.0 equiv) was added, and the reaction mixture was kept in the dark under N_2 and stirred for 10 min. $BF_3 \cdot Et_2O$ (0.7 mL of 1% solution in CH_2Cl_2) was added in one portion, and the mixture was allowed to react at room temperature for 4 h. 2,3-Dichloro-5,6-dicyanobenzoquinone (DDQ, 110 mg, 41.8 mmol, 5.0 equiv) was added to the mixture in one portion, and the mixture was stirred at room temperature for 2 h. The resulting mixture was washed with 10% aqueous Na_2SO_3 (2 × 100 mL) and with water (2 × 100 mL). The combined organic phases were dried over Na_2SO_4. The solvent was evaporated, and the resulting residue was purified by column chromatography on neutral alumina using toluene as eluent. The combined porphyrin mixture was isolated as a green solid with an overall yield of 167 mg (49%).

Synthesis of the Pd(II) Porphyrin Mixture (Scheme 1). An excess of $PdCl_2(PhCN)_2$ (36.0 mg, 0.09 mmol, 2.0 equiv) was added to a solution of porphyrins from the previous procedure (50 mg, 1.0 equiv) in tetrahydrofuran (THF, 20 mL) with triethylamine (1 M), and the mixture was refluxed for 2 h. DDQ (106.0 mg, 0.47 mmol, 10 equiv) was added, and the mixture was refluxed for 1 h. The solvent volume was reduced to 3 mL under vacuum. CH_2Cl_2 (100 mL) was added, and the mixture was washed with aqueous 10% Na_2SO_3. The organic phase was dried over Na_2SO_4, and the solvent was evaporated. The crude product was purified by column chromatography on silica gel (eluent: toluene). The Pd−porphyrin mixture was isolated as a dark-green solid with an overall yield of 34 mg (62%).

Synthesis of the Emitter 3,9(10)-Bis(3,3-dimethylbutyn-1yl)perylene (Scheme 2). The singlet emitter, a π-extended perylene dye, 3,9(10)-bis(3,3-dimethylbutyn-1yl)perylene, was synthesized by bromination of perylene, following the Sonogashira reaction of 3,9(10)-dibromoperylene with 3,3-dimethylbutyne.[64] The 3,9(10)-dibromoperylene (410 mg, 1 mmol), $Pd(PPh_3)_4$ (100 mg), and CuI (30 mg) were added to the mixture of dry THF (15 mL) and dry piperidine (15 mL) in a 100 mL Schlenk flask. The flask was evacuated and flushed with argon several times. A 2-fold molar excess of 3,3-dimethylbutyne (330 mg, 4 mmol) was injected with a syringe. The flask was equipped with a balloon filled with argon and the mixture heated to 50 °C with the stopcock opened. At 50 °C, the stopcock was closed and the temperature was increased to 80 °C. After 14 h at 80 °C, the reaction mixture was poured into a 3-fold volume of ice/HCl (3:1). After standing for 1 h, the yellow precipitate was filtered, rinsed with water, dried under vacuum, and purified by column chromatography on silica gel using toluene/heptane (1:2) as eluent: yield 379 mg (92%); ^{1}H NMR (250 MHz, $C_2D_2Cl_4$, 25 °C, Me_4Si): δ 8.25 (t, J = 7.8 Hz, 2H), 8.18 (d, J = 8.3 Hz, 2H), 8.12 (t, J = 8.0 Hz, 2H), 7.66−7.57 (m, 4H), 1.45 ppm (s, 18H); ^{13}C NMR (75 MHz, $C_2D_2Cl_4$) δ 134.41, 131.03, 130.82, 130.64, 130.58, 130.29, 128.00, 127.11, 127.07, 126.39, 126.28, 121.39, 121.30, 121.01, 120.86, 120.01, 119.87, 105.62, 77.19, 74.15, 74.04, 73.78, 73.41, 31.04 ppm; λ_{max} (toluene)/nm 479 (ε/dm^3 mol^{-1} cm^{-1} 51300), 447 (35500); fluorescence (toluene) λ_{max} = 486 nm (ϕ = 54%, λ_{exc} = 480 nm); MS (FD, 8 kV) m/z (%) 412.1 (100), M$^+$.

Isolation of Nanocellulose. The TEMPO oxidation of pulp was performed as described elsewhere[47] with the modification that 10 mmol of NaClO per gram pulp was used. The oxidized pulp was thoroughly washed with Milli-Q water and disintegrated by two passages through a high-pressure homogenizer (M-110P, Microfludics, U.S.) at 1650 bar and the chamber combination 400/100 μm to obtain TEMPO-oxidized NFC (final solid content of 0.90 wt %). The DP was 440, obtained from intrinsic viscosity measurements.[65]

The blend of short NFC (<1 μm) and CNC used in capsule synthesis was prepared using a new acid hydrolysis route as described elsewhere.[56] The surface charge density of NFC/CNC, due to the presence of carboxylate groups, was 0.031 e nm^{-2} as determined from conductometric titration and by assuming

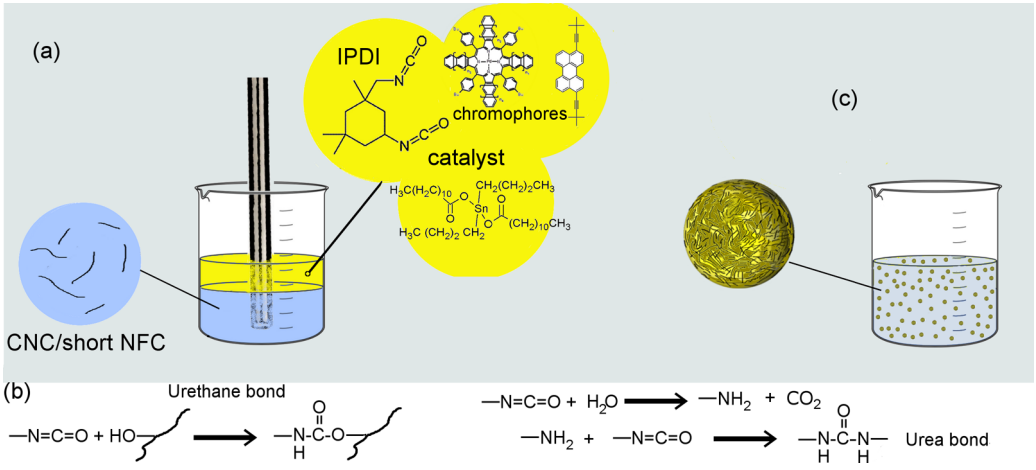

Scheme 3. Illustration of the capsule formation through interfacial polyaddition reaction in the Pickering emulsion.

a cylindrical cross section (density of 1.5 g cm^{-3}) in the calculations.[66,67] Prior to use, this nanocellulose was diluted and flocculates were deaggregated by ultrasonication (Branson Sonifier W-450-Digital with a 1/2 in. tip). A 1 wt % NFC/CNC suspension was obtained by mixing a 0.5 wt % NFC/CNC suspension (70% amplitude, 120 s, ice cooling) with stock suspension (1.71 wt %) and ultrasonicating at 70% amplitude for 2 × 120 s and then 90% amplitude for 60 s under ice cooling. The nanocellulose was 370 ± 210 nm long and 6.7 ± 2.1 nm thick as assessed from AFM height measurements.

Synthesis of Capsules. The synthesis of oil core/nanocellulose shell capsules was performed in direct miniemulsion (see Scheme 3). The capsule wall was created by the reaction between the hydroxyl groups of NFC/CNC and cross-linker (forming urethane bonds) and cross-linker/water (forming urea bonds between cross-linkers) at the O/W interface of oil droplets as described in detail elsewhere.[56] Briefly, the oil phase consisted of 0.7 g of hexadecane, 150 mg of isophorone diisocyanate (cross-linker, IPDI), 25 mg of dibutyltin dilaurate (catalyst needed to increase the reactivity of the isocyanate groups of IPDI), 1×10^{-3} M emitter, and 7×10^{-5} M of the porphyrin mixture. The molar concentrations of each sensitizer in the porphyrin mixture are as follows: Pd-TBP, 12.6×10^{-6} M; Pd-1N3BP, 27.3×10^{-6} M; Pd-2N2BP, 20.3×10^{-6} M; Pd-3NBP, 8.4×10^{-6} M; Pd-TNP, 1.4×10^{-6} M. Then, 6.1 g of a 1 wt % NFC suspension was added to the oil phase and the two phases were mixed together by ultrasonication (Branson Sonifier W-450-Digital with a 1/2 in. tip) at 80% amplitude for 60 s under ice cooling. All emulsions were placed in a heated oil bath at 40 °C, and the polyaddition reaction proceeded under slow magnetic stirring overnight.

Preparation of Films Mounted on Top of Glass. Films were prepared by simple solvent-casting. The suspension of capsules (prepared as described above, capsule content: 13 wt %) and a 0.5 wt % TEMPO-NFC suspension were mixed (ultrasonication at 30% amplitude for 75 s, ice cooling) in a mass ratio of 1:24 and solvent-cast on glass Petri dishes and dried in the dark in a desiccator (with argon atmosphere and drying salt) at ambient temperature. These films adhered strongly to the glass surface. An additional layer on top of these films was created by casting a 0.5 wt % TEMPO-NFC suspension followed by drying in the dark in the same desiccator.

A neat TEMPO-NFC film (used in OTR measurement) was prepared by solvent-casting a 0.5 wt % TEMPO-NFC in a Petri dish (low-density polyethylene) and drying at 40 °C (oven).

The polystyrene film was prepared by dissolving polystyrene (M_W = 890.4 g mol^{-1}) in toluene, in order to obtain at 3.8 wt % solution. Sensitizers and emitter were added in order to obtain 7×10^{-5} and 1×10^{-3} mol dm^{-3}, respectively, in the final dry polystyrene film. The solution was solvent-cast on a glass Petri dish and dried first in the dark at ambient temperature (nitrogen dry glovebox, <1 ppm of O_2) and then overnight in a vacuum oven at 30 °C to remove residual toluene.

Characterization. Unless otherwise stated, the TTA-UC measurements were performed in a chamber with a controllable O_2/N_2 atmosphere. All films (supported on glass Petri dishes) were stored in the dark in a nitrogen dry glovebox (<1 ppm of O_2) for at least 5 days prior to measurements. First, the chamber containing a sample was flushed with nitrogen until virtually all of the oxygen was removed from the sample as noted by the constant level of UC fluorescence. At this point, the oxygen was assumed to be zero both inside and outside the film and the emission $I = I_0$. Afterward, the films was exposed to 1050 mbar dry synthetic air (20.5/79.5 O_2/N_2) at 26.3 ± 0.8 °C, whereupon the oxygen inside the films increased and the measured emission intensity drops. The main direction of oxygen flow into the films is depicted in Figure S5 in Supporting Information. Taking into account that the UC excitation measurement spot was at a macroscopically large distance from the sample edges (2×10^{-2} m), the amount of oxygen penetrated through the sample edges can be neglected (more than 2200 longer pathway). A temperature-stabilized, single-mode continuous-wave diode laser operating at λ = 639 nm and 139 mW cm^{-2} (unless otherwise stated) was used. A series of reflective neutral density filters (Thorlabs Inc.) placed on a revolving optical holder were used to attenuate the beam power. Afterward, the beam was directed through a system of ultra-broad-band mirrors and finally focused by an achromatic lens onto the sample. The luminescence emission was collected with the same achromatic lens, allowing the excitation and observation spots to completely spatially overlap each other. The emission spectra were registered by a CCD spectrometer (C10083CA, Hamamatsu Inc.)

SEM images were taken using a Hitachi SU8000 or a Zeiss Gemini 1530. Capsules were sputter-coated with a 2.5 nm thick Pt coating (Figure 2a). Cross sections of films (Figure 2c) were prepared by bending frozen samples (liquid nitrogen) until fracture. The total thickness of films was assessed from the step height of scratches (obtained with a steel needle) using profilometry (KLA Tencor P-16+). The thickness of the layer containing embedded capsules was obtained by subtracting the thickness of the epidermal layer (assessed from SEM) from the total thickness. Atomic force microscopy images were obtained in tapping mode using a Nanowizard 3 AFM (JPK Instruments, Berlin). The substrate was freshly cleaved mica. Oxygen transmission rate (OTR) was determined according to ASTM standard F2622-08 using a Lyssy OPT-5000 apparatus (PBI-Dansensor, Denmark). Column chromatography was performed on silica gel (Geduran Si60, Merck). HPLC was carried out using Agilent1200 setup at room temperature (pump and photodiodes array detector (DAD); column Agilent Eclipse Plus C18, L = 100 mm/diameter = 4.6 mm/particle size = 3−5 μm, λ = 260 nm, eluent gradient starting THF/methanol = 5:95 up to 60:40 with 1 mL min^{-1}). ^1H and ^{13}C NMR spectra were recorded on Bruker DPX 250 and Bruker Avance 300 spectrometers. FD mass spectra were measured with a VG Instruments ZAB

2-SE-FPD instrument. UV/vis spectra were recorded on a PerkinElmer Lambda 900 spectrophotometer. Fluorescence spectra were recorded on a Spex Fluorolog 3 spectrometer. Fluorescence quantum yields of emitter were determined by the relative method using Acridine Yellow as a reference (η = 47% in ethanol). The upconversion setup is described elsewhere.[23]

Conflict of Interest: The authors declare no competing financial interest.

Acknowledgment. Dr. M. Henriksson is acknowledged for performing the intrinsic viscosity measurements, and Assoc. Prof. J. Risbo is acknowledged for reading through the manuscript. Prof. P. Ulvskov is acknowledged for valuable discussion. Funding was provided by Reintegration Grant RG-09-0002(DRG-02/2) Bulgarian National Science Fund (S.B.) and the Danish Council for Independent Research (A.J.S.).

Supporting Information Available: The structure of the individual sensitizers, HPLC chromatogram and individual absorption spectra of the synthesized porphyrin ensemble, gas flow direction in films, SEM images of nanocellulose-based capsules, and capsule wall thickness. This material is available free of charge *via* the Internet at http://pubs.acs.org.

REFERENCES AND NOTES

1. Baluschev, S.; Miteva, T.; Yakutkin, V.; Nelles, G.; Yasuda, A.; Wegner, G. Up-conversion Fluorescence: Noncoherent Excitation by Sunlight. *Phys. Rev. Lett.* **2006**, *97*, No. 143903.
2. Islangulov, R. R.; Lott, J.; Weder, C.; Castellano, F. N. Noncoherent Low-Power Upconversion in Solid Polymer Films. *J. Am. Chem. Soc.* **2007**, *129*, 12652–12653.
3. Baluschev, S.; Yakutkin, V.; Miteva, T.; Avlasevich, Y.; Chernov, S.; Aleshchenkov, S.; Nelles, G.; Cheprakov, A.; Yasuda, A.; Mullen, K.; *et al.* Blue-Green Up-conversion: Noncoherent Excitation by NIR Light. *Angew. Chem., Int. Ed.* **2007**, *46*, 7693–7696.
4. Keivanidis, P. E.; Baluschev, S.; Miteva, T.; Nelles, G.; Scherf, U.; Yasuda, A.; Wegner, G. Up-conversion Photoluminescence in Polyfluorene Doped with Metal(II)-Octaethyl Porphyrins. *Adv. Mater.* **2003**, *15*, 2095–2098.
5. Islangulov, R. R.; Kozlov, D. V.; Castellano, F. N. Low Power Upconversion Using MLCT Sensitizers. *Chem. Commun.* **2005**, 3776–3778.
6. Baluschev, S.; Jacob, J.; Avlasevich, Y. S.; Keivanidis, P. E.; Miteva, T.; Yasuda, A.; Nelles, G.; Grimsdale, A. C.; Mullen, K.; Wegner, G. Enhanced Operational Stability of the Upconversion Fluorescence in Films of Palladium-Porphyrin End-Capped Poly(pentaphenylene). *ChemPhysChem* **2005**, *6*, 1250–1253.
7. Schulze, T. F.; Czolk, J.; Cheng, Y. Y.; Fuckel, B.; MacQueen, R. W.; Khoury, T.; Crossley, M. J.; Stannowski, B.; Lips, K.; Lemmer, U.; *et al.* Efficiency Enhancement of Organic and Thin-Film Silicon Solar Cells with Photochemical Upconversion. *J. Phys. Chem. C* **2012**, *116*, 22794–22801.
8. Baluschev, S.; Yakutkin, V.; Wegner, G.; Miteva, T.; Nelles, G.; Yasuda, A.; Chernov, S.; Aleshchenkov, S.; Cheprakov, A. Upconversion with Ultrabroad Excitation Band: Simultaneous Use of Two Sensitizers. *Appl. Phys. Lett.* **2007**, *90*, No. 181103.
9. Singh-Rachford, T. N.; Castellano, F. N. Pd(II) Phthalocyanine-Sensitized Triplet−Triplet Annihilation from Rubrene. *J. Phys. Chem. A* **2008**, *112*, 3550–3556.
10. Singh-Rachford, T. N.; Haefele, A.; Ziessel, R.; Castellano, F. N. Boron Dipyrromethene Chromophores: Next Generation Triplet Acceptors/Annihilators for Low Power Upconversion Schemes. *J. Am. Chem. Soc.* **2008**, *130*, 16164–16165.
11. Miteva, T.; Yakutkin, V.; Nelles, G.; Baluschev, S. Annihilation Assisted Upconversion: All-Organic, Flexible and Transparent Multicolour Display. *New J. Phys.* **2008**, *10*, No. 103002.
12. Chen, H. C.; Hung, C. Y.; Wang, K. H.; Chen, H. L.; Fann, W. S.; Chien, F. C.; Chen, P. L.; Chow, T. J.; Hsu, C. P.; Sun, S. S. White-Light Emission from an Upconverted Emission with an Organic Triplet Sensitizer. *Chem. Commun.* **2009**, 4064–4066.
13. Singh-Rachford, T. N.; Castellano, F. N. Triplet Sensitized Red-to-Blue Photon Upconversion. *J. Phys. Chem. Lett.* **2010**, *1*, 195–200.
14. Ji, S. M.; Wu, W. H.; Wu, W. T.; Guo, H. M.; Zhao, J. Z. Ruthenium(II) Polyimine Complexes with a Long-Lived (IL)-I-3 Excited State or a (MLCT)-M-3/(IL)-I-3 Equilibrium: Efficient Triplet Sensitizers for Low-Power Upconversion. *Angew. Chem., Int. Ed.* **2011**, *50*, 1626–1629.
15. Murakami, Y.; Kikuchi, H.; Kawai, A. Kinetics of Photon Upconversion in Ionic Liquids: Energy Transfer between Sensitizer and Emitter Molecules. *J. Phys. Chem. B* **2013**, *117*, 2487–2494.
16. Kim, J. H.; Deng, F.; Castellano, F. N.; Kim, J. H. High Efficiency Low-Power Upconverting Soft Materials. *Chem. Mater.* **2012**, *24*, 2250–2252.
17. Wang, Q.; Oswald, I. W. H.; Perez, M. R.; Jia, H. P.; Gnade, B. E.; Omary, M. A. Exciton and Polaron Quenching in Doping-Free Phosphorescent Organic Light-Emitting Diodes from a Pt(II)-Based Fast Phosphor. *Adv. Funct. Mater.* **2013**, *23*, 5420–5428.
18. Zou, W. Q.; Visser, C.; Maduro, J. A.; Pshenichnikov, M. S.; Hummelen, J. C. Broadband Dye-Sensitized Upconversion of Near-Infrared Light. *Nat. Photonics* **2012**, *6*, 560–564.
19. Borjesson, K.; Dzebo, D.; Albinsson, B.; Moth-Poulsen, K. Photon Upconversion Facilitated Molecular Solar Energy Storage. *J. Mater. Chem. A* **2013**, *1*, 8521–8524.
20. Kim, J. H.; Kim, J. H. Encapsulated Triplet−Triplet Annihilation-Based Upconversion in the Aqueous Phase for Sub-band-Gap Semiconductor Photocatalysis. *J. Am. Chem. Soc.* **2012**, *134*, 17478–17481.
21. Liu, Q.; Yang, T. S.; Feng, W.; Li, F. Y. Blue-Emissive Upconversion Nanoparticles for Low-Power-Excited Bioimaging *in Vivo*. *J. Am. Chem. Soc.* **2012**, *134*, 5390–5397.
22. Borisov, S. M.; Saf, R.; Fischer, R.; Klimant, I. Synthesis and Properties of New Phosphorescent Red Light-Excitable Platinum(II) and Palladium(II) Complexes with Schiff Bases for Oxygen Sensing and Triplet−Triplet Annihilation-Based Upconversion. *Inorg. Chem.* **2013**, *52*, 1206–1216.
23. Turshatov, A.; Busko, D.; Baluschev, S.; Miteva, T.; Landfester, K. Micellar Carrier for Triplet−Triplet Annihilation-Assisted Photon Energy Upconversion in a Water Environment. *New J. Phys.* **2011**, *13*, No. 083035.
24. Kang, J. H.; Reichmanis, E. Low-Threshold Photon Upconversion Capsules Obtained by Photoinduced Interfacial Polymerization. *Angew. Chem., Int. Ed.* **2012**, *51*, 11841–11844.
25. Wohnhaas, C.; Turshatov, A.; Mailander, V.; Lorenz, S.; Baluschev, S.; Miteva, T.; Landfester, K. Annihilation Upconversion in Cells by Embedding the Dye System in Polymeric Nanocapsules. *Macromol. Biosci.* **2011**, *11*, 772–778.
26. Simon, Y. C.; Bai, S.; Sing, M. K.; Dietsch, H.; Achermann, M.; Weder, C. Low-Power Upconversion in Dye-Doped Polymer Nanoparticles. *Macromol. Rapid Commun.* **2012**, *33*, 498–502.
27. Wu, W. H.; Guo, H. M.; Wu, W. T.; Ji, S. M.; Zhao, J. Z. Organic Triplet Sensitizer Library Derived from a Single Chromophore (BODIPY) with Long-Lived Triplet Excited State for Triplet−Triplet Annihilation Based Upconversion. *J. Org. Chem.* **2011**, *76*, 7056–7064.
28. Singh-Rachford, T. N.; Lott, J.; Weder, C.; Castellano, F. N. Influence of Temperature on Low-Power Upconversion in Rubbery Polymer Blends. *J. Am. Chem. Soc.* **2009**, *131*, 12007–12014.
29. Monguzzi, A.; Bianchi, F.; Bianchi, A.; Mauri, M.; Simonutti, R.; Ruffo, R.; Tubino, R.; Meinardi, F. High Efficiency Upconverting Single Phase Elastomers for Photon Managing Applications. *Adv. Energy. Mater.* **2013**, *3*, 680–686.
30. Lee, S. H.; Lott, J. R.; Simon, Y. C.; Weder, C. Melt-Processed Polymer Glasses for Low-Power Upconversion *via* Sensitized Triplet−Triplet Annihilation. *J. Mater. Chem. C* **2013**, *1*, 5142–5148.
31. Merkel, P. B.; Dinnocenzo, J. P. Low-Power Green-to-Blue and Blue-to-UV Upconversion in Rigid Polymer Films. *J. Lumin.* **2009**, *129*, 303–306.

32. Merkel, P. B.; Dinnocenzo, J. P. Experimental and Theoretical Study of Triplet Energy Transfer in Rigid Polymer Films. *J. Phys. Chem. A* **2008**, *112*, 10790–10800.
33. Monguzzi, A.; Tubino, R.; Meinardi, F. Multicomponent Polymeric Film for Red to Green Low Power Sensitized Up-conversion. *J. Phys. Chem. A* **2009**, *113*, 1171–1174.
34. Monguzzi, A.; Frigoli, M.; Larpent, C.; Tubino, R.; Meinardi, F. Low-Power-Photon Up-conversion in Dual-Dye-Loaded Polymer Nanoparticles. *Adv. Funct. Mater.* **2012**, *22*, 139–143.
35. Liu, Q.; Yin, B. R.; Yang, T. S.; Yang, Y. C.; Shen, Z.; Yao, P.; Li, F. Y. A General Strategy for Biocompatible, High-Effective Upconversion Nanocapsules Based on Triplet–Triplet Annihilation. *J. Am. Chem. Soc.* **2013**, *135*, 5029–5037.
36. Kim, J. H.; Deng, F.; Castellano, F. N.; Kim, J. H. Red-to-Blue/Cyan/Green Upconverting Microcapsules for Aqueous- and Dry-Phase Color Tuning and Magnetic Sorting. *ACS Photonics* **2014**, *1*, 382–388.
37. Simon, Y. C.; Weder, C. Low-Power Photon Upconversion through Triplet–Triplet Annihilation in Polymers. *J. Mater. Chem.* **2012**, *22*, 20817–20830.
38. Lu, X.; Winnik, M. A. Luminescence Quenching in Polymer/Filler Nanocomposite Films Used in Oxygen Sensors. *Chem. Mater.* **2001**, *13*, 3449–3463.
39. Litvinov, V. M.; Persyn, O.; Miri, V.; Lefebvre, J. M. Morphology, Phase Composition, and Molecular Mobility in Polyamide Films in Relation to Oxygen Permeability. *Macromolecules* **2010**, *43*, 7668–7679.
40. Huang, J.; Zhu, H.; Chen, Y.; Preston, C.; Rohrbach, K.; Cumings, J.; Hu, L. Highly Transparent and Flexible Nanopaper Transistors. *ACS Nano* **2013**, *7*, 2106–2113.
41. Korhonen, J. T.; Hiekkataipale, P.; Malm, J.; Karppinen, M.; Ikkala, O.; Ras, R. H. A. Inorganic Hollow Nanotube Aerogels by Atomic Layer Deposition onto Native Nanocellulose Templates. *ACS Nano* **2011**, *5*, 1967–1974.
42. Wang, J.; Cheng, Q.; Lin, L.; Jiang, L. Synergistic Toughening of Bioinspired Poly(vinyl alcohol)–Clay–Nanofibrillar Cellulose Artificial Nacre. *ACS Nano* **2014**, *8*, 2739–2745.
43. Zhu, H.; Li, Y.; Fang, Z.; Xu, J.; Cao, F.; Wan, J.; Preston, C.; Yang, B.; Hu, L. Highly Thermally Conductive Papers with Percolative Layered Boron Nitride Nanosheets. *ACS Nano* **2014**, *8*, 3606–3613.
44. Hamedi, M. M.; Hajian, A.; Fall, A. B.; Håkansson, K.; Salajkova, M.; Lundell, F.; Wågberg, L.; Berglund, L. A. Highly Conducting, Strong Nanocomposites Based on Nanocellulose-Assisted Aqueous Dispersions of Single-Wall Carbon Nanotubes. *ACS Nano* **2014**, *8*, 2467–2476.
45. Karabulut, E.; Pettersson, T.; Ankerfors, M.; Wågberg, L. Adhesive Layer-by-Layer Films of Carboxymethylated Cellulose Nanofibril–Dopamine Covalent Bioconjugates Inspired by Marine Mussel Threads. *ACS Nano* **2012**, *6*, 4731–4739.
46. Walther, A.; Timonen, J. V. I.; Diez, I.; Laukkanen, A.; Ikkala, O. Multifunctional High-Performance Biofibers Based on Wet-Extrusion of Renewable Native Cellulose Nanofibrils. *Adv. Mater.* **2011**, *23*, 2924–2928.
47. Fukuzumi, H.; Saito, T.; Iwamoto, S.; Kumamoto, Y.; Ohdaira, T.; Suzuki, R.; Isogai, A. Pore Size Determination of TEMPO-Oxidized Cellulose Nanofibril Films by Positron Annihilation Lifetime Spectroscopy. *Biomacromolecules* **2011**, *12*, 4057–4062.
48. Saito, T.; Kuramae, R.; Wohlert, J.; Berglund, L. A.; Isogai, A. An Ultrastrong Nanofibrillar Biomaterial: The Strength of Single Cellulose Nanofibrils Revealed *via* Sonication-Induced Fragmentation. *Biomacromolecules* **2013**, *14*, 248–253.
49. Alexandrescu, L.; Syverud, K.; Gatti, A.; Chinga-Carrasco, G. Cytotoxicity Tests of Cellulose Nanofibril-Based Structures. *Cellulose* **2013**, *20*, 1765–1775.
50. Aulin, C.; Gallstedt, M.; Lindstrom, T. Oxygen and Oil Barrier Properties of Microfibrillated Cellulose Films and Coatings. *Cellulose* **2010**, *17*, 559–574.
51. Buchanan, B. B.; Gruissem, W.; Jones, R. L. *Biochemistry & Molecular Biology of Plants*; American Society of Plant Physiologists: Rockville, MD, 2000.
52. Schweitzer, C.; Schmidt, R. Physical Mechanisms of Generation and Deactivation of Singlet Oxygen. *Chem. Rev.* **2003**, *103*, 1685–1757.
53. Svagan, A. J.; Akesson, A.; Cardenas, M.; Bulut, S.; Knudsen, J. C.; Risbo, J.; Plackett, D. Transparent Films Based on PLA and Montmorillonite with Tunable Oxygen Barrier Properties. *Biomacromolecules* **2012**, *13*, 397–405.
54. Svagan, A. J.; Hedenqvist, M. S.; Berglund, L. Reduced Water Vapour Sorption in Cellulose Nanocomposites with Starch Matrix. *Compos. Sci. Technol.* **2009**, *69*, 500–506.
55. Hess, S.; Demir, M. M.; Yakutkin, V.; Baluschev, S.; Wegner, G. Investigation of Oxygen Permeation through Composites of PMMA and Surface-Modified ZnO Nanoparticles. *Macromol. Rapid Commun.* **2009**, *30*, 394–401.
56. Svagan, A. J.; Musyanovych, A.; Kappl, M.; Bernhardt, M.; Glasser, G.; Wohnhaas, C.; Berglund, L. A.; Risbo, J.; Landfester, K. Cellulose Nanofiber/Nanocrystal Reinforced Capsules: A Fast and Facile Approach toward Assembly of Liquid-Core Capsules with High Mechanical Stability. *Biomacromolecules* **2014**, *15*, 1852–1859.
57. Pickering, S. U. Emulsions. *J. Chem. Soc.* **1907**, *91*, 2001–2021.
58. Henriksson, M.; Berglund, L. A.; Isaksson, P.; Lindstrom, T.; Nishino, T. Cellulose Nanopaper Structures of High Toughness. *Biomacromolecules* **2008**, *9*, 1579–1585.
59. Wu, W. H.; Zhao, J. Z.; Guo, H. M.; Sun, J. F.; Ji, S. M.; Wang, Z. L. Long-Lived Room-Temperature Near-IR Phosphorescence of BODIPY in a Visible-Light-Harvesting N C N PtII-Acetylide Complex with a Directly Metalated BODIPY Chromophore. *Chem.—Eur. J.* **2012**, *18*, 1961–1968.
60. Zhao, J. Z.; Wu, W. H.; Sun, J. F.; Guo, S. Triplet Photosensitizers: From Molecular Design to Applications. *Chem. Soc. Rev.* **2013**, *42*, 5323–5351.
61. Borisov, S. M.; Larndorfer, C.; Klimant, I. Triplet–Triplet Annihilation-Based Anti-Stokes Oxygen Sensing Materials with a Very Broad Dynamic Range. *Adv. Funct. Mater.* **2012**, *22*, 4360–4368.
62. Baluschev, S.; Miteva, T. Non-coherent Up-Conversion in Multi-component Organic Systems. In *Next Generation of Photovoltaics*; Cristóbal López, A. B., Martí Vega, A., Luque López, A., Eds.; Springer: Berlin, 2012; Vol. 165, pp 157–190.
63. Niedermair, F.; Borisov, S. M.; Zenkl, G.; Hofmann, O. T.; Weber, H.; Saf, R.; Klimant, I. Tunable Phosphorescent NIR Oxygen Indicators Based on Mixed Benzo- and Naphthoporphyrin Complexes. *Inorg. Chem.* **2010**, *49*, 9333–9342.
64. Schlichting, P.; Rohr, U.; Mullen, K. New Synthetic Routes to Alkyl-Substituted and Functionalized Perylenes. *Liebigs Ann./Recl.* **1997**, 395–407.
65. Svagan, A. J.; Jensen, P.; Dvinskikh, S. V.; Furo, I.; Berglund, L. A. Towards Tailored Hierarchical Structures in Cellulose Nanocomposite Biofoams Prepared by Freezing/Freeze-Drying. *J. Mater. Chem.* **2010**, *20*, 6646–6654.
66. Saito, T.; Isogai, A. TEMPO-Mediated Oxidation of Native Cellulose. The Effect of Oxidation Conditions on Chemical and Crystal Structures of the Water-Insoluble Fractions. *Biomacromolecules* **2004**, *5*, 1983–1989.
67. Jiang, F.; Esker, A. R.; Roman, M. Acid-Catalyzed and Solvolytic Desulfation of H_2SO_4-Hydrolyzed Cellulose Nanocrystals. *Langmuir* **2010**, *26*, 17919–17925.